


Coherence of Velocity Fluctuations in Turbulent Flows

G. Prabhudesai[✉], S. Perrard[✉], F. Pétrélis, and S. Fauve*Laboratoire de Physique de l'École Normale Supérieure, CNRS, PSL Research University, Sorbonne Université, Université de Paris, F-75005 Paris, France* (Received 25 July 2021; revised 26 October 2021; accepted 8 December 2021; published 4 January 2022)

We investigate the spatiotemporal quantity of coherence for turbulent velocity fluctuations at spatial distances of the order or larger than the integral length scale l_0 . Using controlled laboratory experiments, an exponential decay as a function of distance is observed with a decay rate that depends on the flow properties. The same law is observed in two different flows, indicating that it can be a generic property of turbulent flows.

DOI: 10.1103/PhysRevLett.128.014501

Introduction.—Part of the spatial structure of turbulent flows has been extensively studied owing to the concept of energy cascade by Richardson [1] and later extended to a scale invariant hypothesis in Kolmogorov's 1941 theory [2]. In a three dimensional turbulent flow, a direct cascade of energy takes place between the integral length scale l_0 associated to the energy injection scale and the Kolmogorov length scale η where energy gets eventually dissipated. In contrast, the spatiotemporal properties of velocity fluctuations in turbulent flows for separation distance r comparable to or larger than the integral length scale l_0 have been significantly less studied. Yet, understanding the behavior of turbulent fluctuations at large scales is not only of fundamental interest, it also has application for instance in geophysical or astrophysical flows when a large scale field bifurcates over a small scale turbulent flow [3]. Magnetic field generation by the alpha effect of astrophysical dynamos [4] and large scale hydrodynamic flow generated by the anisotropic kinetic alpha effect of helical flows [5] are two examples in which fluctuations at small scales may affect a large scale field, in particular if these fluctuations display some coherent behavior at large temporal or spatial scales. The statistical properties of the large scales of turbulent flows are also of interest in industrial applications such as wind turbine farms for instance (see below).

One tool to study the spatiotemporal velocity fluctuations at large scales in an homogeneous, stationary turbulent flow is the magnitude squared coherence or simply coherence defined from the signal at two points separated by vector \mathbf{r} and a time lag τ as

$$\mathcal{C}(\mathbf{r}, f) = \frac{|E_{ij}(\mathbf{r}, f)|^2}{E_i(f)E_j(f)}, \quad (1)$$

where $E_{ij}(\mathbf{r}, f) = \int_{-\infty}^{\infty} \langle u_i(\mathbf{x}, t) u_j(\mathbf{x} + \mathbf{r}, t + \tau) \rangle e^{if\tau} d\tau$ is the cross spectrum and $E_i(f) = \int_{-\infty}^{\infty} \langle u_i(\mathbf{x}, t) u_i(\mathbf{x}, t + \tau) \rangle e^{if\tau} d\tau$

the one point spectrum of the i th component. Coherence may refer to different velocity components. We denote in particular longitudinal (respectively transverse) coherence function with $i = j$ and the velocity component parallel (respectively perpendicular) to \mathbf{r} .

In the context of turbulent atmospheric boundary layer, a few field experiments and modeling approaches have been devoted to the study of coherence [6–11] to estimate power load fluctuations in wind turbine farms [12,13] or to evaluate large scale constraints on bridges [14] and buildings [15]. The coherence function is, however, still poorly documented, with measurements only in the context of the turbulent atmospheric boundary layer and turbulent wakes.

Despite $\mathcal{C}(\mathbf{r}, f)$ being a standard quantity in signal analysis, it has been rarely used for turbulent data even though it provides additional information about two-point correlation functions at equal time to which it is related but not in a simple way.

In this Letter, we investigate the behavior of coherence in two controlled laboratory experiments that we design to either vary the typical timescale or length scale of the flow. In both setups, we also achieve a large separation of length scale between the size of the experimental domain and the integral length scale l_0 .

Experimental setup and results.—The first experimental setup is sketched in Fig 1(a). Four pairs of helices are mounted on vertical bars immersed in a cubical tank of size 15 cm. Set in rotation by loop-controlled motors at an angular velocity Ω , the helices force the flow directly in the bulk. The four axes are rotated in a clockwise direction and Ω ranges from 0 to 3200 rpm. In order to obtain full optical access, we implement an index matching technique. We 3D print the helices in a transparent resin (Nano Clear) of refractive index $n = 1.51$, and we match the resin refractive index by using a liquid mixture of 62% in volume of anise oil and 38% in volume of mineral oil. As suggested by Song *et al.* [16], the anise and mineral oil mixture is particularly suitable for optical measurements of flows as a

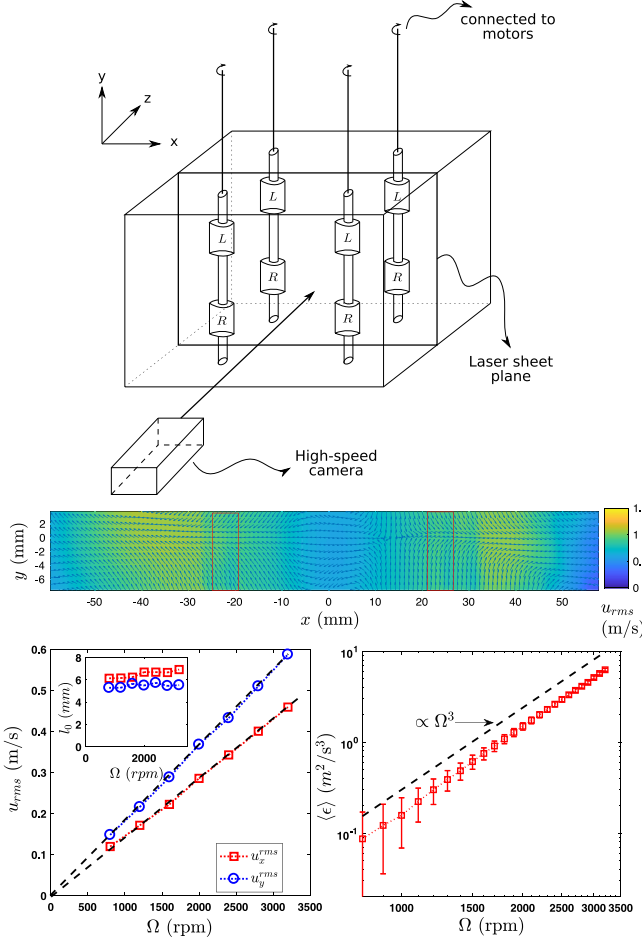


FIG. 1. (a) Sketch of the experimental setup composed of 8 helices mounted on four vertical bars (R and L stand for right and left chirality). The velocity field is measured in the central xy plane using the PIV technique. (b) 2D map of the magnitude of velocity fluctuations u_{rms} . The blue arrows indicate the local direction of the mean flow, which evidence the stagnation point at the center. The positions of the vertical bars are indicated in red. (c) rms of velocity fluctuation along x (Squared box) and along y (Circle). Inset: longitudinal integral length scale l_0 along x (Squared box) and y (Circle). (d) Global mean energy injection rate per unit mass $\langle \epsilon \rangle$ evaluated from the motor power consumption.

highly transparent, low viscosity ($\nu = 4.5$ cP for 62% anise oil) fluid. We perform optical velocity measurements using both laser Doppler anemometry and particle image velocimetry (PIV). The laser Doppler anemometry apparatus, composed of a precalibrated Dantec system, is used to characterize the local properties of the flow at small scale, while the PIV is used to study the large scale spatiotemporal fluctuations. The PIV is performed on vertical planes using a high-speed camera and a continuous 2 W laser of wavelength 532 nm. Using a combination of two spherical lenses and two cylindrical lenses, we obtain a vertical laser sheet with a tunable angle of divergence and a thickness of 500 μm in the tank. Particles of diameter

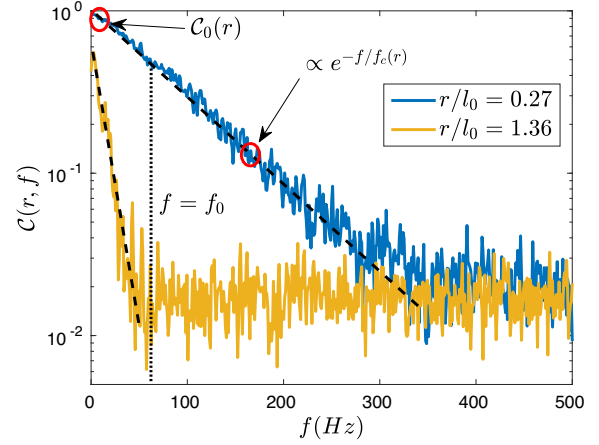


FIG. 2. Coherence as a function of frequency measured for $\Omega = 3200$ rpm at two spatial distances: $r/l_0 = 0.27$ (blue line) and $r/l_0 = 1.36$ (yellow line).

$30 \pm 10 \mu\text{m}$ are seeded in the flow, and the velocity field is reconstructed from the images using a free PIV algorithm [17]. Figure 1(b) shows the map of the two dimensional root mean squared velocity $u_{\text{rms}}^{\text{tot}} = \sqrt{(u_x^{\text{rms}})^2 + (u_y^{\text{rms}})^2}$ averaged over time. The blue arrow indicated the direction of the mean flow, showing the stagnation point at the center of the tank. This mean flow is, however, smaller than the velocity fluctuations in the region of interest. The rms of velocity fluctuations u_{rms} along x and y varies linearly with the rotation rate [Fig. 1(c)]. The correlation length of velocity fluctuations is computed using the two-point spatial correlation at equal time, which displays an exponential decay with a characteristic length defined as the integral length scale l_0 . The integral length scale is measured to be independent of Ω (Fig. 1(c) inset) for the range of rotation rates studied with $l_0 = 6 \pm 1$ mm being significantly smaller than the box size. We measure the mean energy injection rate per unit mass $\langle \epsilon \rangle$ from the power required by the motors to maintain the flow. We find that $\langle \epsilon \rangle \propto \Omega^3$ [Fig. 1(d)], which confirms that we reach the large scale scaling at high Reynolds number $\langle \epsilon \rangle = C_\epsilon u_{\text{rms}}^3 / l_0$ with the dimensionless constant $C_\epsilon = 0.4$ [18,19]. The rms of one velocity component is denoted by u_{rms} , whose scaling can also be recovered from dimensional arguments in the limit of high Reynolds number. Eventually, we estimate the Taylor Reynolds number $\text{Re}_\lambda = u_{\text{rms}} \lambda / \nu$, where λ is the Taylor microscale associated to the correlation length of velocity gradients, which can be estimated from u_{rms} and the dissipation rate, equal to the mean injection rate $\langle \epsilon \rangle$ in a statistically stationary regime. For the highest rotation speed, we achieve a Taylor Reynolds number $\text{Re}_\lambda \approx 100$ and $\lambda \approx 1$ mm.

We focus on the large scale behavior corresponding to r of the order or larger than l_0 . Unless otherwise stated, measurements are reported for $r/l_0 \geq 0.27$. Figure 2 shows coherence for the longitudinal component of the velocity as

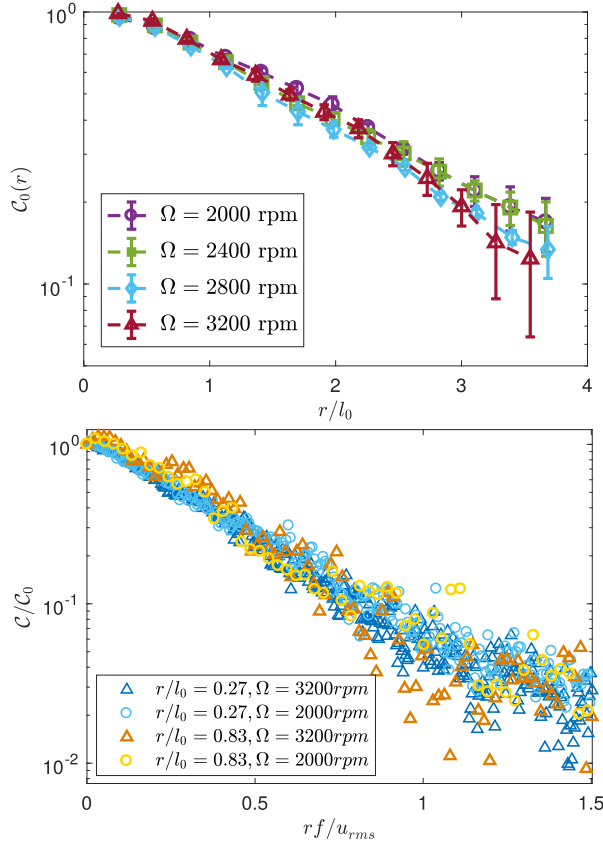


FIG. 3. (a) Coherence at zero frequency C_0 as a function of the dimensionless distance r/l_0 . (b) Normalized coherence C/C_0 as a function of the dimensionless frequency rf/u_{rms} .

a function of frequency for two different values of distance r at $\Omega = 3200$ rpm. We observe an exponential decay $C = C_0(r) \exp(-f/f_c)$, where f_c^{-1} is the decay rate in frequency and C_0 the coherence at zero frequency. Both C_0 and f_c are observed to decay with r . Their values are evaluated from the least rms error exponential fit of C from 1 to the noise level at large frequencies. The decay of C_0 with r/l_0 is shown in Fig. 3(a), each curve corresponding to a different value of Ω . We find an exponential decay of C_0 with a characteristic length scale proportional to the integral length scale l_0 .

These measurements imply that $C_0 = \exp(-c_1 r/l_0)$. Further analysis on the frequency dependence of coherence reveals $f_c = c_2 u_{rms}/r$, where u_{rms} is the rms of the longitudinal component of velocity. This can be seen in Fig. 3(b), where coherence normalized by its value at zero frequency is plotted against normalized frequency rf/u_{rms} for two different values of r and of Ω . The four curves lie within a single master curve. The experimentally observed behavior of coherence is hence of the form

$$C(r, f) = \exp(-c_1 r/l_0) \exp(-c_2 rf/u_{rms}), \quad (2)$$

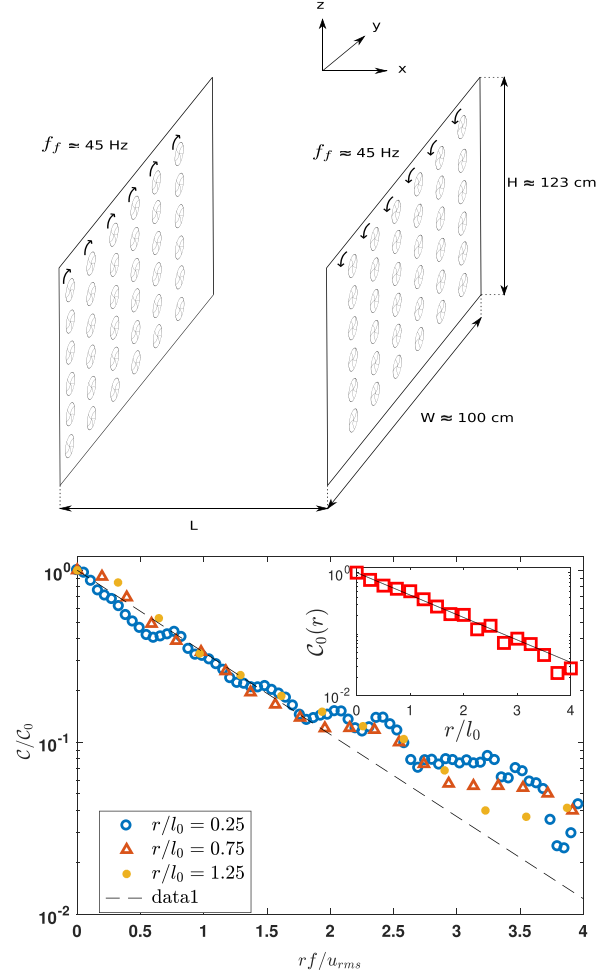


FIG. 4. (a) Sketch of the experimental setup of two walls of counter-rotating staggered fans. Each wall is fitted with 36 fans. (b) Normalized coherence C/C_0 as a function of rf/u_{rms} . Inset: coherence C_0 at zero frequency as a function of the dimensionless distance r/l_0 . C/C_0 and C_0 exhibit exponential decay, respectively, in rf/u_{rms} and r/l_0 .

with $c_1 = 0.54$ and $c_2 = 2.5$, valid for $r/l_0 \geq 0.27$. This functional form remains valid for the transverse component of velocity.

In this first experiment, however, the integral length scale does not vary significantly. To further check the relation $C_0 = \exp(-r/l_0)$, we design a second experiment where a turbulent flow is generated in air between two square walls (length 1 m) of counter-rotating staggered fans. A sketch of the setup is shown in Fig. 4(a). This configuration creates a Roberts-like turbulent flow [20] between the two walls. We use two 1D hot-wire probes using constant temperature anemometry technique to measure the two-point spatio-temporal quantities of speed fluctuations near the center. We vary the distance between the walls from 20 to 80 cm, which modifies the integral scale l_0 of the flow from 1.5 to 3.5 cm. Concomitantly, the rms of velocity fluctuations u_{rms} ranges from 0.1 to 0.5 m/s. We get a maximum Taylor

Reynolds number $Re_\lambda \approx 100$ for the minimum wall distance, corresponding to an integral length scale $l_0 \sim O(1)$ cm. The coherence \mathcal{C} in this setup also exhibits an exponential decay of the form given by Eq. (2), as shown in Fig. 4(b), with $c_1 = 0.84$ and $c_2 = 1.1$. The value of c_1 is found to be similar between the two experiments. The value of c_2 is likely underestimated in the second experiment due to the hot-wire technique, which evaluates the speed of the sum of longitudinal and one transverse velocity component instead of the longitudinal velocity. The two experimental configurations confirm the functional form of \mathcal{C} of Eq. (2) and in particular the dependency on the integral length scale l_0 that can here be varied.

Physical interpretation.—In a homogeneous flow, coherence is an even function of r . Assuming that viscous effects render the flow properties smooth at small enough distances, coherence is expected to be quadratic in r at small r . By definition it is equal to 1 at $r = 0$. Tobin and Chamorro [21] used the random sweeping hypothesis as formulated by Tennekes [22] and Kraichnan [23] to model the phase fluctuations of velocity cross spectrum in the presence of a mean flow. In the limit of large mean flow U compared to the velocity fluctuations, they predicted $\mathcal{C}(r, f) \propto \exp(-cr^2f^2/U^2)$. For non-negligible velocity fluctuations compared to the mean velocity, there is no prediction for the behavior of coherence. Though, in the context of spatiotemporal correlation function of temperature fluctuations in Rayleigh Bénard convection, an elliptic approximation has been developed using Taylor hypothesis [24,25]. The experiments that we report here are designed to study the behavior for $r \geq l_0$. Our results at small r are compatible with a quadratic behavior, but even for r/l_0 of the order of $1/4$ we observe that the frequency dependence of coherence has the form $\mathcal{C}(r, f) \propto \exp(-crf/u_{\text{rms}})$, thus decaying slower than the prediction from the random sweeping hypothesis.

An exponential decay in coherence implies that the relation between coherence at r and $r + \Delta$ is given by $C(r + \Delta, f) = C(r, f)g(\Delta)$, where g is a function that only depends on the separation distance Δ . In other words, such a behavior implies a memoryless process for coherence. It is interesting to note that a similar behavior is observed in the context of temporal correlation for Markovian process, though no direct relation exists between the two. The local functional relation on $C(r + \Delta, f)$ leads to the existence of a spatial correlation length Γ^{-1} , characterizing the exponential decay of the form $C(r, f) \propto \exp(-\Gamma r)$. Our measurements show that

$$\Gamma = \frac{c_1 f}{u_{\text{rms}}} + \frac{c_2}{l_0}. \quad (3)$$

This exponential behavior of the coherence takes place at separation distance r not too small, i.e., when the sweeping effect of the turbulent fluctuations has lost its coherence.

The form of the correlation length Γ^{-1} interpolates between the injection length scale at small f and u_{rms}/f at large f .

We note that among the different empirical models introduced for coherence in turbulent atmospheric boundary layers, an exponential decay in the vertical coordinate is usually considered with a prefactor that depends on frequency. This is, for instance, the case of the Davenport model as later refined by Thresher *et al.* $\mathcal{C}(z, f) \propto \exp(-\sqrt{a(zf/U)^2 + (bz/L)^2})$ [6,7,9], with U the horizontal mean flow velocity, L a characteristic length, and a and b numerical constants. The asymptotic behavior at small or large f is similar to our results of Eq. (2) even though the contexts are different: specific role played by the vertical coordinate, presence of a strong mean flow that renders Taylor's hypothesis valid, and the consideration of only the inertial scales.

Conclusion.—We have shown experimentally that at scales larger than a fraction of the integral scale (for $r/l_0 \geq 0.27$), the coherence of the velocity in a turbulent flow decays exponentially in frequency and in space with a decay rate of the form of Eq. (3). Being observed in two different experimental setups, we believe that our observations are generic to the large scales of turbulent flows.

This work has been supported by the Agence nationale de la recherche (Grant No. ANR-17-CE30-0004) and CEFIPRA (Project No. 6104-1).

*Corresponding author.

gaurav.prabhudesai@ens.fr

- [1] L. F. Richardson, *Weather Prediction by Numerical Process* (Cambridge University Press, Cambridge, England, 2007), ISBN 9780521680448.
- [2] A. N. Kolmogorov, The local structure of turbulence in incompressible viscous fluid for very large Reynolds numbers, *Dokl. Akad. Nauk SSSR* **30**, 301 (1941).
- [3] S. Fauve, J. Hérault, G. Michel, and F. Pétrélis, Instabilities on a turbulent background, *J. Stat. Mech.* **2017**, 064001 (2017).
- [4] H. K. Moffatt, *Magnetic Field Generation in Electrically Conducting Fluids* (Cambridge University Press, Cambridge, England, 1978), ISBN 978-0521216401.
- [5] U. Frisch, Z. She, and P. Sulem, Large-scale flow driven by the anisotropic kinetic alpha effect, *Physica (Amsterdam)* **28D**, 382 (1987).
- [6] A. G. Davenport, The spectrum of horizontal gustiness near the ground in high winds, *Q. J. R. Meteorol. Soc.* **87**, 194 (1961).
- [7] R. W. Thresher, W. E. Holley, C. E. Smith, N. Jafarey, and S.-R. Lin, Modeling the response of wind turbines to atmospheric turbulence, Technical Report No. RL0/2227-81/2, Department of Mechanical Engineering, Oregon State University, 1981.
- [8] L. Kristensen and N. O. Jensen, Lateral coherence in isotropic turbulence and in the natural wind, *Boundary-Layer Met.* **17**, 353 (1979).

- [9] K. Saranyasontorn, L. Manuel, and P. S. Veers, A comparison of standard coherence models for inflow turbulence with estimates from field measurements, *J. Solar Energy Eng.* **126**, 1069 (2004).
- [10] C. J. Baker, Wind engineering: Past, present and future, *J. Wind Eng. Ind. Aerodyn.* **95**, 843 (2007).
- [11] D. Krug, W. J. Baars, N. Hutchins, and I. Marusic, Vertical coherence of turbulence in the atmospheric surface layer: Connecting the hypotheses of townsend and davenport, *Boundary-Layer Meteorol.* **172**, 199 (2019).
- [12] L. J. Vermeer, J. N. Sorensen, and A. Crespo, Wind turbine wake aerodynamics, *Prog. Aerosp. Sci.* **39**, 467 (2003).
- [13] P. Sorensen, N. A. Cutululis, A. Viguera-Rodriguez, H. Madsen, P. Pinson, L. E. Jensen, J. Hjerrild, and M. Donovan, Power fluctuations from large wind farms, *IEEE Transactions on Power Systems; IEEE Transactions on Power Electronics* **22**, 958 (2007).
- [14] E. Cheynet, J. B. Jakobsen, and J. Snaebjornsson, Buffeting response of a suspension bridge in complex terrain, *Engineering structures* **128**, 474 (2016).
- [15] E. Simiu and R. Scanlan, *Wind Effects on Structures: Fundamentals and Applications to Design* (Wiley, New York, 1996).
- [16] M. S. Song, H. Y. Choi, J. H. Seong, and E. S. Kim, Matching-index-of-refraction of transparent 3d printing models for flow visualization, *Nucl. Eng. Des.* **284**, 185 (2015).
- [17] W. Thielicke and E. J. Stamhuis, PIVlab—towards user-friendly, affordable and accurate digital particle image velocimetry in MATLAB, *J. Open Res. Software* **2**, e30 (2014).
- [18] S. B. Pope, *Turbulent Flows* (Cambridge University Press, Cambridge, England, 2000), ISBN 9780521598866.
- [19] J. C. Vassilicos, Dissipation in turbulent flows, *Annu. Rev. Fluid Mech.* **47**, 95 (2015).
- [20] G. O. Roberts, Dynamo action of fluid motions with two-dimensional periodicity, *Phil. Trans. R. Soc. A* **271**, 411 (1972).
- [21] N. Tobin and L. P. Chamorro, Turbulence coherence and its impact on wind-farm power fluctuations, *J. Fluid Mech.* **855**, 1116 (2018).
- [22] H. Tennekes, Eulerian and lagrangian time microscales in isotropic turbulence, *J. Fluid Mech.* **67**, 561 (1975).
- [23] S. Chen and R. H. Kraichnan, Sweeping decorrelation in isotropic turbulence, *Phys. Fluids A* **1**, 2019 (1989).
- [24] X. He, G. He, and P. Tong, Small-scale turbulent fluctuations beyond taylor’s frozen-flow hypothesis, *Phys. Rev. E* **81**, 065303(R) (2010).
- [25] A. Kumar and M. K. Verma, Applicability of taylor’s hypothesis in thermally driven turbulence, *R. Soc. Open Sci.* **5**, 172152 (2018).